Double conical crystal x-ray spectrometer for high resolution ultrafast x-ray absorption near-edge spectroscopy of $\mathrm{Al}\,K$ edge

A. Levy, F. Dorchies, C. Fourment, M. Harmand, S. Hulin, J. J. Santos, D. Descamps, S. Petit, and R. Bouillaud

Citation: Review of Scientific Instruments **81**, 063107 (2010); doi: 10.1063/1.3441983
View online: https://doi.org/10.1063/1.3441983
View Table of Contents: http://aip.scitation.org/toc/rsi/81/6
Published by the American Institute of Physics

Double conical crystal x-ray spectrometer for high resolution ultrafast x-ray absorption near-edge spectroscopy of Al *K* edge

A. Levy, F. Dorchies,[a] C. Fourment, M. Harmand, S. Hulin, J. J. Santos, D. Descamps, S. Petit, and R. Bouillaud
Centre Lasers Intenses et Applications (CELIA), Université de Bordeaux-CNRS-CEA, Talence F-33405, France

(Received 22 January 2010; accepted 10 May 2010; published online 17 June 2010)

An x-ray spectrometer devoted to dynamical studies of transient systems using the x-ray absorption fine spectroscopy technique is presented in this article. Using an ultrafast laser-induced x-ray source, this optical device based on a set of two potassium acid phthalate conical crystals allows the extraction of x-ray absorption near-edge spectroscopy structures following the Al absorption *K* edge. The proposed experimental protocol leads to a measurement of the absorption spectra free from any crystal reflectivity defaults and shot-to-shot x-ray spectral fluctuation. According to the detailed analysis of the experimental results, a spectral resolution of 0.7 eV rms and relative fluctuation lower than 1% rms are achieved, demonstrated to be limited by the statistics of photon counting on the x-ray detector. © *2010 American Institute of Physics.* [doi:10.1063/1.3441983]

I. INTRODUCTION

The rapid progress of laboratory ultrafast x-ray source development opens new possibilities for different applications requiring a dynamical study of various processes in a large panel of scientific disciplines from condensed matter physics to chemistry, or biology.[1] An ultrashort x-ray emission can be achieved with different kinds of techniques such as laser-produced plasmas,[2] high harmonic radiation,[3] and laser-induced betatron sources.[4] Although the average photon brilliance of these sources is still weaker than the emissions offered at conventional synchrotrons, they present different important advantages. More recently, the upcoming x-ray free electron laser installations offer narrowband x-ray sources presenting the advantage of an intense photon brilliance coupled with a short duration of the emission.[5]

The specific case of x-ray radiation obtained by the interaction of an intense ultrashort laser pulse with a solid target generates considerable interest due to the very compact size and relatively low cost of this kind of installation. In addition, in a case of pump-probe experiment and for all laser-induced x-ray sources, one can easily use the same laser pulse to trigger the transient system which is studied and the x-ray probe, enabling the synchronization at a femtosecond time scale. Finally, this emission presents the advantage of a short duration, down to the picosecond or subpicosecond domain.[1] For these reasons, this kind of x-ray source is developed for different available time-resolved x-ray probe techniques. Among them we can mention various works devoted to use x-ray diffraction for the study of laser-heated organic films,[6] lattice dynamics in crystals,[7] phase transitions,[8,9] and taking advantage of x-ray line emission emitted from laser irradiated solid targets. Another technique based on these sources optimized for a broadband spectral emission is the x-ray absorption fine spectroscopy (XAFS).[10] The latter has attracted considerable attention as a tool for investigating the short-range order of the atomic arrangement and electronic state density of a wide variety of amorphous systems.[11]

This XAFS technique has already been developed by different groups which had designed various kinds of spectrometers adapted to a specific energy range dependent on the studied system.[12–15] Several experiments have been recently performed taking advantage of this technique for the study of different dynamical processes: laser-shock compression of materials,[16] chemical reactions,[17] and solid-liquid-plasma phase transitions,[18–20] to cite only a few. In each case, the characteristics required for the spectrometer are fixed by the energy range of interest and the parameters of the laser facility, as for example the repetition rate. In this paper, we describe an x-ray spectrometer devoted to XAFS experiments in the keV range designed for the study of solid to plasma phase transition. For this purpose, we have previously optimized an x-ray source using the broadband thermal emission from a high *Z* plasma[21] taking advantage of *M*-shell transitions. The feasibility of x-ray absorption experiment has been already reported in Ref. 22, demonstrating the interest of such a source for the study of the atomic structure of a solid sample.

In this work, we present a spectrometer and the experimental protocol designed to achieve Al *K*-edge x-ray absorption fine spectroscopy. Based on a set of two conical potassium acid phthalate (KAP) crystals, this optical device greatly enhances the detected photon flux and releases the results from the shot-to-shot fluctuations of the x-ray source. A detailed analysis of the measurements is reported demonstrating that, in these experimental conditions, the fluctuations on the absorption spectra are sufficiently low to enable a precise extraction of the x-ray absorption near-edge spectroscopy (XANES) structures.

[a]Electronic mail: dorchies@celia.u-bordeaux1.fr.

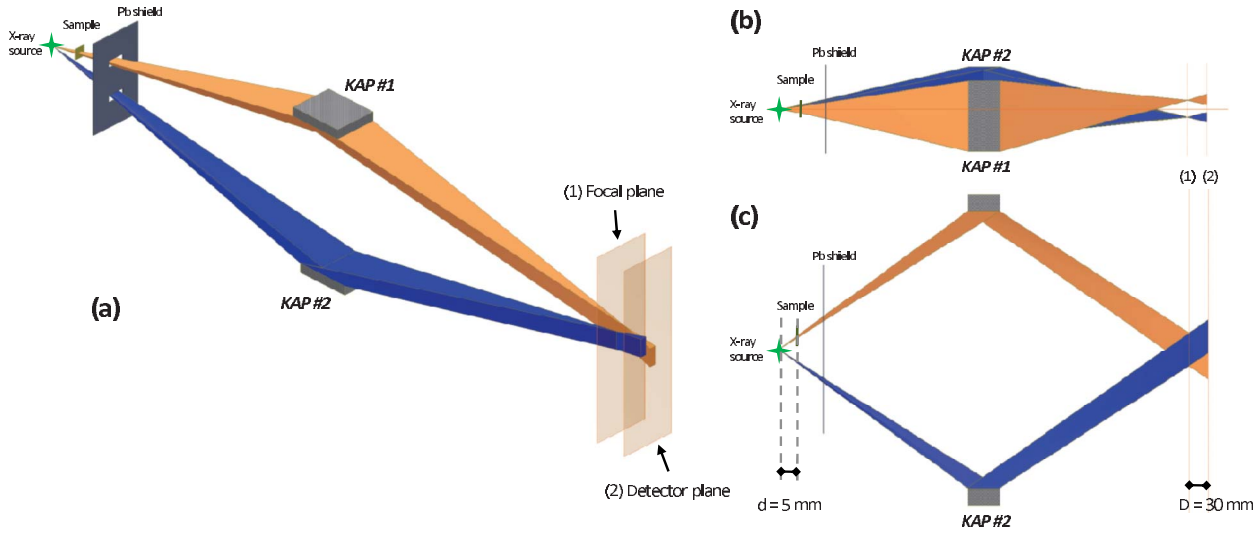

FIG. 1. (Color online) Schematic view of the x-ray spectrometer: (a) three-dimensional representation, (b) top view, and (c) side view.

II. X-RAY SPECTROMETER DESIGN

The experimental characterization of the x-ray spectrometer has been performed on the 1 kHz Aurore Ti:sapphire laser system at Centre Lasers Intenses et Applications (CELIA). It delivers 30 fs pulses with an energy of 5 mJ at a central wavelength of 800 nm. By the use of an $f/4$ lens, the laser beam is focused up to an intensity of 10^{17} W/cm^2 on a thick erbium target to generate the desired x-ray source. As reported in a previous publication,[21] we have accomplished a systematic study of this source, and a compromise has been found to maximize the signal-to-noise ratio (10^4:1), the photon flux ($\simeq 10^7$ photons/shot sr eV) in the energy range of the Al K-edge (between $\sim$1.5 and 1.7 keV), and minimize the x-ray pulse duration ($\simeq$3–4 ps) as a function of laser parameters and target material.

The spectrometer collects the x-ray emission in an energy range from 1.5 to 1.7 keV limited by the size of the detector. Represented in Fig. 1, it uses two conically bent KAP crystals. This crystal geometry, first proposed by Hall *et al.*,[23] is achieved by bending the crystal on a surface corresponding to a cone such as the apex is positioned in the focal plane. The main interest of this geometry is the focusing of the signal in a segment orthogonal to the detection axis.[24] The crystals we used are characterized by the following parameters: a dimension of 50×30 mm^2, the cone half angle $\theta_{\text{apex}}=0.3$ rad, and the upper and lower radii of curvature are, respectively, 96.04 and 81.27 mm. The crystals are positioned at a distance of 92.8 mm of the horizontal plane containing the x-ray source and, in consequence, their alignment is optimized to focus the signal in a plane at a distance of 60 cm from the source.

As represented in Fig. 1, the spectrometer is composed of a set of two identical crystal symmetrically positioned on both sides of the detection axis which connects the x-ray source to the detector. In addition, a slight lateral translation is introduced between them to avoid the overlapping of the two traces in the detection plane. This translation is however sufficiently small to enable the collection of the two spectra on a single detector. Using such spectrometer configuration, one can easily record simultaneously the direct emission of the x-ray source (KAP 2) as well as the transmitted spectrum through a sample (KAP 1) just placing it in the collection angle of the corresponding crystal.

Finally, the detector used in this case is a 16 bit charge-coupled device (CCD) camera directly illuminated. This device allows a direct measurement of the number of detected x-ray photons using a calibration law function of the photon energy (1.6 keV photon $\simeq$49 CCD counts). We placed the CCD camera 3 cm ($=D$) away from the focal plane in order to achieve a spatial resolution of the sample imaging which leads to a magnification for these parameters of $\gamma=-D/d=-6$ (where d is defined as the distance of the sample from the x-ray source and is equal in our case to 5 mm). The use of a conical crystal in this point projection geometry[18] is very attractive since it allows a magnification adjustment just moving the detector away from the focal plane, without changing the wavelength range. In addition, a given wavelength corresponds to a line perpendicular to the spectral dispersion in the detection plane. The spatial resolution is limited by three main factors. The first one is related to the pixel size of the camera: 24 μm (i.e., 4 μm in the sample plane). The second one which is estimated around 100 μm (i.e., 17 μm) is due to x-ray conical crystal aberrations.[25] However, in the case presented here, the main limitation is induced by the x-ray source size ($\simeq$50 μm) leading to a resolution in the sample plane of 40 μm. The spectral resolution is also limited by different contributions which are maximized by the imperfection of the lattice due to its stretching and compression. This leads to a spectral resolution ranging from 1.5 to 3 eV according to Ref. 24. In addition, the spectral resolution due to the vertical extension of the x-ray source is estimated around 0.73 eV and the contribution of the fluctuation of the x-ray position due to variation in the laser pointing is in the order of 0.15 eV. Finally, the last limitation which we can consider is related to the pixel size of the CCD detector and leads to a spectral resolution of 0.35 eV.

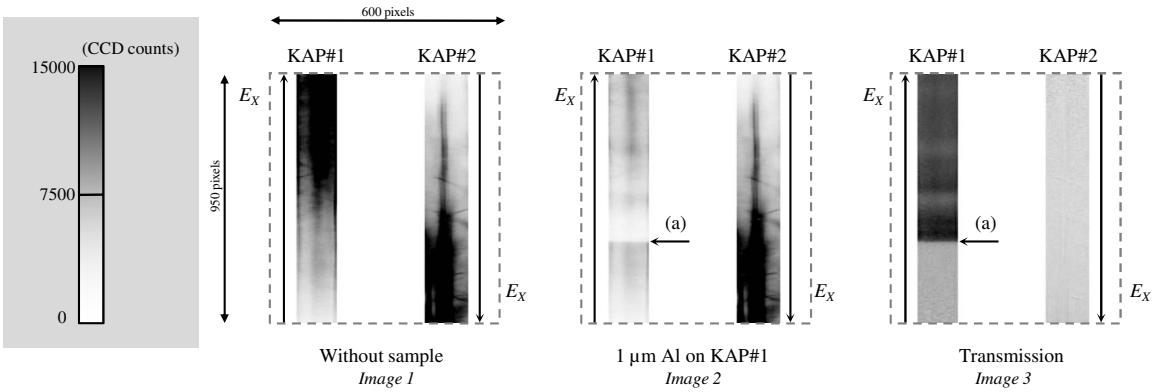

FIG. 2. Experimental protocol: (left=image 1) reference spectra recorded without Al sample; (middle=image 2) typical spectra collected with a 1 μm thick Al sample in front of the KAP 1; (right=image 3) calculated ratio image 2/image 1. The energy axis (E_x) of the two crystals is oriented in opposite directions due to the geometry of the spectrometer. The arrow (a) indicates the Al absorption K edge. The spatial scale of the images is indicated for the first one and is identical for the others. The grayscale reported on the left indicates the magnitude of the signal of the images 1 and 2.

Finally, the detector is shielded from the direct emission of the source with a 1 mm thick Pb foil. To prevent the crystals from any debris coming from the laser-matter interaction, we placed a thin polypropylene foil (4 μm) which did not significantly modify the collected signal. In this energy range, the transmission of this film is uniform and estimated at about 80%–85%.

The method to retrieve the absorption features from these x-ray spectra measurements is described in the next section. We performed these measurements for various aluminum foil thicknesses from 1000 Å to 2 μm.

III. ABSORPTION SPECTRA EXTRACTION

All the results obtained with this x-ray absorption spectrometer have been measured accumulating the signal over 20 s at 1 kHz repetition rate. The typical results presented in the Fig. 2 have been obtained with 1 μm thick Al foil. The vertical axis corresponds to the photon energy dispersion and the horizontal one to the spatial dimension.

To deduce the absorption spectrum, we established a precise experimental protocol illustrated in Fig. 2. First, we recorded a reference image (image 1) with no Al sample revealing the defaults of KAP crystals reflectivity. The second step consists in recording the spectra with the sample in front of the KAP 1 (image 2) comparable to the first image but exhibiting the Al K-edge on the corresponding crystal [see arrow (a) in Fig. 2]. In addition, one can notice that, as expected, thanks to the conical crystal geometry, the absorption edge is perpendicular to the spectral dispersion axis. Calculating the ratio of these two images, we have access to the transmission of the sample on KAP 1 and the shot-to-shot fluctuation of the x-ray source is registered on the image corresponding to KAP 2 (image 3). Both spectra are released from the crystal reflectivity defaults. However, the transmission of the sample in this case (left part of the image 3) is still influenced by the shot-to-shot fluctuation. Dividing this image by the transmission with no sample (right part of the image 3), one can obtain the absolute transmission released from this specific fluctuation.

The photon number $N_{i,j}$ detected in the image j (j=1: without sample; j=2: with a sample in front of the KAP 1) and collected with KAP i is given by the following equation:

$$N_{i,j} = R_i S_j T_{i,j}. \tag{1}$$

R_i includes the spatial reflectivity of the crystal i, the corresponding solid angle of detection, and the detection efficiency of the CCD camera. S_j is the x-ray signal emitted by the source during the registering of the image j. $T_{i,j}$ is the transmission coefficient of the sample. In other words, $T_{1,2}=T$ represents the transmission of the probed aluminum foil and the others $T_{i,j}=1$. The transmission T is then deduced from the $N_{i,j}$ measurements using the following equation:

$$T = \frac{N_{1,2}}{N_{1,1}} \frac{N_{2,1}}{N_{2,2}}. \tag{2}$$

In this equation, the first factor represents the transmission of the sample free of the crystal reflectivity defaults since $(N_{1,2}/N_{1,1})=(S_2T/S_1)$ (left part of image 3). The second one, $(N_{2,1}/N_{2,2})=(S_1/S_2)$, is a correction factor to get rid of the shot-to-shot fluctuation of the x-ray source (right part of image 3).

The linear absorption coefficient μ is then directly deduced using the relation $A=\mu d=-\ln(T)$, where A is the absorbance of the sample and d its thickness. The corresponding spectrum, integrated over the spatial dimension, is reported in Fig. 3. In the case of this experiment, the sharp-

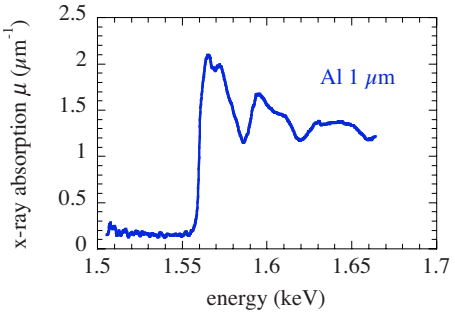

FIG. 3. (Color online) X-ray absorption spectrum of 1 μm thick Al sample deduced from the measurements presented in Fig. 2.

ness of the cold absorption edge is limited by the achieved spectral resolution. According to the measurement reported in Fig. 3, we determined that the absorption spectra are convolved with an experimental Gaussian resolution of 1.7 eV full width at half maximum, i.e., 0.7 eV rms in agreement with the theoretical estimation given above.

This result demonstrates the feasibility of extracting the XANES structures of the absorption spectrum in such experimental conditions. This observation is detailed in the next section.

IV. MEASUREMENT ACCURACY

The main interest of this technique lies in the possibility to extract spectra free from any reflectivity defaults of the crystals included in R_i and from the shot-to-shot variations in the x-ray source (S_j) which allows accurate absorption measurements. However, we can distinguish other sources of noise which can be estimated. First, the CCD camera can induce a fluctuation on the measurement but reduced to a negligible value (a few CCD counts) if one uses an appropriate cooling ($\simeq -35$ °C) of the device. Second, fluctuation on the absorption spectra can be related to the statistical fluctuation of the x-ray photon number detected. In our case, this term is dominant and we present in this section an experimental analysis of this contribution, its impact on the absorption results, and a comparison of this measured fluctuation with a simple model. However, in some cases, a nonnegligible source of noise (hard x rays) independent of the x-ray spectrometer can come into play due to the laser-matter interaction itself. For the measurements presented here, this component has been reduced thanks to an optimization of the x-ray source and in consequence will not be taken into account.

To estimate the contribution due the statistical fluctuation of the photon number, we consider that the photon number $N_{i,j}$ detected follows a binomial probability law. In addition, due to the small collection angle of the crystals, one can assume a weak probability for one x-ray photon to be detected by the CCD camera. According to this, one can demonstrate that the standard deviation (rms) $\delta N_{i,j}$ on this measurement is given by $\delta N_{i,j}=\sqrt{N_{i,j}}$. As a consequence, we found an induced fluctuation δA_0 on the absorbance without the Al sample (i.e., $\langle T_0\rangle=1$ and $\langle A_0\rangle=0$) that can be estimated using the following equation:

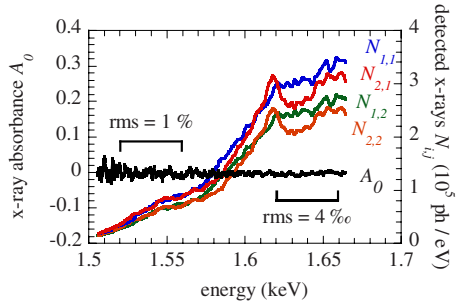

FIG. 4. (Color online) Fluctuation measurement on x-ray absorbance spectra in a case without sample: spectra $N_{i,j}$ measured on image j collected by KAP i and the corresponding absorbance spectrum A_0. All these spectra are recorded with an accumulation time of 20 s at 1 kHz repetition rate.

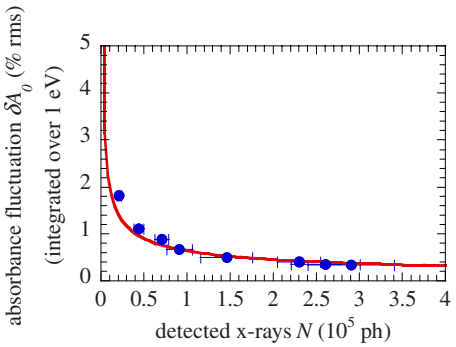

FIG. 5. (Color online) Fluctuation δA_0 measured on x-ray absorbance spectrum A_0 without sample vs the number of photon N detected on CCD. Data registered (circles) vs calculation (line).

$$\delta A_0 = \sqrt{\sum_{i,j}\left(\frac{1}{\sqrt{N_{i,j}}}\right)^2} \approx \frac{2}{\sqrt{N}}, \tag{3}$$

where N is the mean photon number detected on each image and KAP.

To confirm this theoretical evaluation of the statistical fluctuation, we compared it with measurements. In Fig. 4, we reported the spectra of the detected x-ray photons $N_{i,j}$ and the corresponding absorbance A_0 without sample. As expected the mean value of the absorbance spectrum is equal to 0 and the standard deviation of the fluctuations increases with a decreasing photon number. In Fig. 5, this feature is represented and compared to Eq. (3). The excellent agreement validates the model.

However, the key parameter of this study is the absorption μ (strictly speaking the linear absorption in μm^{-1}). In Fig. 6, we present different experimental measurements of the absorption spectra as function of Al thickness d. The fluctuation expected on the spectra strongly depends on the target thickness d and increases for a 1000 Å Al foil compared to a thicker one. In consequence, the capability to extract the XAFS structures from the experimental spectra will be reduced in the case of a thin target and a compromise has to be found between this limitation and the rapid decrease in the photon number detected after the absorption edge for an increasing target thickness.

To analyze this point, we generalized the estimation of the expected fluctuation to the case with an Al sample and we demonstrated that the statistical relative fluctuation of the absorption is given by the following equation:

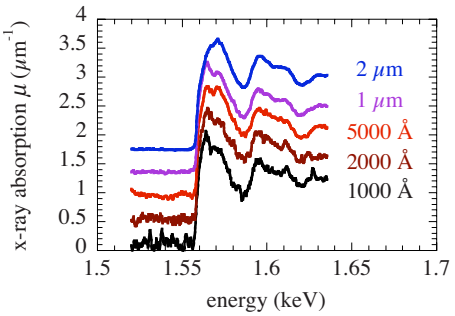

FIG. 6. (Color online) Experimental linear absorption coefficient vs photon energy, for different sample thicknesses. The different curves have been artificially shifted on the vertical axis for clarity reasons.

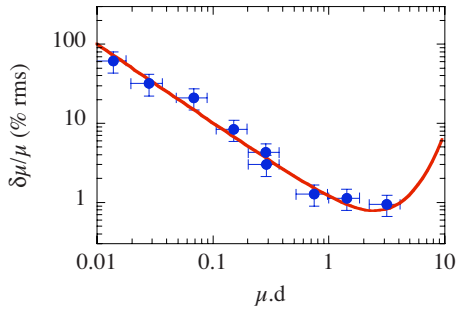

FIG. 7. (Color online) Relative fluctuation measurements $\delta\mu/\mu$ on x-ray absorption spectra vs the absorbance $A=\mu d$. Data registered (circles) vs calculation (line).

$$\frac{\delta\mu}{\mu} = \delta A_0 \frac{\sqrt{3+\exp(\mu d)}}{2\mu d}, \tag{4}$$

where we recognize the fluctuation on the absorbance δA_0 for a case without Al sample.

This equation is illustrated in Fig. 7 and compared to the experimental measurements. These measurements have been obtained averaging the results of Fig. 6 over two spectral ranges (1.53–1.55 and 1.6–1.61 keV) for the various Al sample thicknesses. Thereby, we have been able to estimate the relative fluctuation $\delta\mu/\mu$ for a wide panel of the absorbance $A=\mu d$. As expected and observed in Fig. 6, this relative fluctuation is reduced by several orders of magnitude for an increasing target thickness. However, this is valid for a value of the product μd not greater than $\simeq 3$ beyond which the fluctuations will strongly increase. One can in addition note that the comparison of the experimental results and the theoretical curve reveals an excellent agreement. Finally, this optimal value of μd found in this study is close to the one reported in Refs. 26 and 27.

For the specific case of the experiment presented in this paper, the absorbance in the energy range of the XAFS structures is approximately equal to 1.4 for the 1 μm target. According to the results presented before, this Al thickness is in consequence the optimal one we can obtain for this x-ray flux and with a acceptable relative fluctuation lower than 1% rms.

V. CONCLUSION

In conclusion, we have presented in this paper an x-ray spectrometer and the experimental protocol devoted to probe the structural dynamics of transient systems in the energy range of the Al absorption K edge. Taking advantage of high Z plasma M-shell broadband emission, we extracted the XANES features of a cold aluminum sample to demonstrate the feasibility of such experiment. This spectrometer achieves a spectral resolution of 0.7 eV rms and we demonstrated that the relative statistical fluctuations can be reduced to approximately 1% rms mainly limited by the number of detected photons. This spectrometer has been coupled with a 1 kHz laser induced x-ray source for this paper but can be used with a single shot laser facility as long as the x-ray photon number detected by the CCD camera is sufficient. In addition, such a study can be easily generalized to a larger spectral range just adapting the KAP crystals of the spectrometer. Finally, this diagnostic has been already used in an experiment dedicated to a dynamical study of the warm dense matter regime and reported in Ref. 28.

ACKNOWLEDGMENTS

The authors would like to thank C. Medina for her precious help on the laser, as well A. Tempel for their technical assistance. This work is partially supported by the Fond Européen de Développement Economique Régional and the Conseil Régional d'Aquitaine.

[1] T. Pfeifer, C. Spielmann, and G. Gerber, Rep. Prog. Phys. **69**, 443 (2006).
[2] H. Schwoerer, Top. Appl. Phys. **96**, 237 (2004).
[3] E. Seres, J. Seres, and C. Spielmann, Appl. Phys. Lett. **89**, 181919 (2006).
[4] A. Rousse, K. Ta Phuoc, R. Shah, A. Pukhov, E. Lefebvre, V. Malka, S. Kiselev, F. Burgy, J.-P. Rousseau, D. Umstadter, and D. Hulin, Phys. Rev. Lett. **93**, 135005 (2004).
[5] S. Khan, J. Mod. Opt. **55**, 3469 (2008).
[6] C. Rischel, A. Rousse, I. Uschmann, P.-A. Albouy, J.-P. Geindre, P. Audebert, J.-C. Gauthier, E. Forster, J.-L. Martin, and A. Antonetti, Nature (London) **390**, 490 (1997).
[7] C. Rose-Petruck, R. Jimenez, T. Guo, A. Cavalleri, C. W. Siders, F. Raksi, J. A. Squier, B. C. Walker, K. R. Wilson, and C. P. J. Barty, Nature (London) **398**, 310 (1999).
[8] K. Sokolowski-Tinten, C. Blome, C. Dietrich, A. Tarasevitch, M. Horn von Hoegen, D. von der Linde, A. Cavalleri, J. Squier, and M. Kammler, Phys. Rev. Lett. **87**, 225701 (2001).
[9] A. Cavalleri, Cs. Toth, C.W. Siders, J. A. Squier, F. Raksi, P. Forget, and J. C. Kieffer, Phys. Rev. Lett. **87**, 237401 (2001).
[10] P. Forget, F. Dorchies, J.-C. Kieffer, and O. Peyrusse, Chem. Phys. **299**, 259 (2004).
[11] C. Bressler and M. Chergui, Chem. Rev. (Washington, D.C.) **104**, 1781 (2004).
[12] U. Vogt, T. Wilhein, H. Stiel, and H. Legall, Rev. Sci. Instrum. **75**, 4606 (2004).
[13] S. Fourmaux, L. Lecherbourg, M. Harmand, M. Servol, and J.-C. Kieffer, Rev. Sci. Instrum. **78**, 113104 (2007).
[14] S. L. Johnson, P. A. Heimann, M. Lindenberg, H. O. Jeschke, M. E. Garcia, Z. Chang, R. W. Lee, J. J. Rehr, and R. W. Falcone, Phys. Rev. Lett. **91**, 157403 (2003).
[15] Y. Okano, K. Oguri, T. Nishikawa, and H. Nakano, Rev. Sci. Instrum. **77**, 046105 (2006).
[16] B. Yaakobi, T. R. Boehly, T. C. Sangster, D. D. Meyerhofer, B. A. Remington, P. G. Allen, S. M. Pollaine, H. E. Lorenzana, K. T. Lorenz, and J. A. Hawreliak, Phys. Plasmas **15**, 062703 (2008).
[17] F. Ráksi, K. R. Wilson, Z. Jiang, A. Ikhlef, C. Y. Côté, and J.-C. Kieffer, J. Chem. Phys. **104**, 6066 (1996).
[18] P. Audebert, P. Renaudin, S. Bastiani-Ceccotti, J.-P. Geindre, C. Chenais-Popovics, S. Tzortzakis, V. Nagels-Silvert, R. Shepherd, I. Matsushima, S. Gary, F. Girard, O. Peyrusse, and J.-C. Gauthier, Phys. Rev. Lett. **94**, 025004 (2005).
[19] S. L. Johnson, P. A. Heimann, A. G. MacPhee, A. M. Lindenberg, O. R. Monteiro, Z. Chang, R. W. Lee, and R. W. Falcone, Phys. Rev. Lett. **94**, 057407 (2005).
[20] K. Oguri, Y. Okano, T. Nishikawa, and H. Nakano, Phys. Rev. Lett. **99**, 165003 (2007).
[21] M. Harmand, F. Dorchies, O. Peyrusse, D. Descamps, C. Fourment, S. Hulin, S. Petit, and J. J. Santos, Phys. Plasmas **16**, 063301 (2009).
[22] F. Dorchies, M. Harmand, D. Descamps, C. Fourment, S. Hulin, S. Petit, O. Peyrusse, and J. J. Santos, Appl. Phys. Lett. **93**, 121113 (2008).
[23] T. A. Hall, J. Phys. E **17**, 110 (1984).
[24] E. Martinolli, M. Koenig, J. M. Boudenne, E. Perelli, D. Batani, and T. A. Hall, Rev. Sci. Instrum. **75**, 2024 (2004).
[25] C. Bonté, M. Harmand, F. Dorchies, S. Magnan, V. Pitre, J.-C. Kieffer, P. Audebert, and J. P. Geindre, Rev. Sci. Instrum. **78**, 043503 (2007).
[26] E. A. Stern and K. Kim, Phys. Rev. B **23**, 3781 (1981).
[27] M. E. Rose and M. M. Shapiro, Phys. Rev. **74**, 1853 (1948).
[28] A. Lévy, F. Dorchies, M. Harmand, C. Fourment, S. Hulin, O. Peyrusse, J. J. Santos, P. Antici, P. Audebert, J. Fuchs, L. Lancia, A. Mancic, M. Nakatsutsumi, S. Mazevet, V. Recoules, P. Renaudin, and S. Fourmaux, Plasma Phys. Controlled Fusion **51**, 124021 (2009).